# Role of Hydroperoxyl Radicals in Heterogeneous Oxidation of Oxygenated Organic Aerosols

Wen Zhang[1], Kassem Issa[2], Tiffany Tang[1], Haofei Zhang[1]*

[1]Department of Chemistry, University of California, Riverside, California 92507, USA

[2]Department of Evolution, Ecology, and Organismal Biology, University of California, Riverside, California 92507, USA

*Corresponding Author. Email: haofei.zhang@ucr.edu

**Abstract**

Heterogeneous oxidative aging of organic aerosols (OA) occurs ubiquitously in the atmosphere, initiated by oxidants such as the hydroxyl radicals (•OH). Hydroperoxyl radicals ($HO_2^•$) are also important oxidant in the troposphere and its gas-phase chemistry has been well studied. However, the role of $HO_2^•$ in heterogeneous OA oxidation remains elusive. Here, we carry out •OH-initiated heterogeneous oxidation of several OA model systems under different $HO_2^•$ conditions in a flow tube reactor and characterize the molecular oxidation products using a suite of mass spectrometry instrumentation. By using hydrogen-deuterium exchange with thermal desorption iodide-adduct chemical ionization mass spectrometry, we provide direct observation of organic hydroperoxide (ROOH) formation from heterogeneous $HO_2^•$ and peroxy radicals ($RO_2^•$) reactions for the first time. The ROOH may contribute substantially to the oxidation products, varied with the parent OA chemical structure. Furthermore, by regulating $RO_2^•$ reaction pathways, $HO_2^•$ also greatly influence the overall composition of the oxidized OA. Lastly, we suggest that the $RO_2^• + HO_2^•$ reactions readily occur at the OA particle interface rather than in the particle bulk. These findings provide new mechanistic insights into the heterogeneous OA oxidation chemistry and help fill the critical knowledge gap in understanding atmospheric OA oxidative aging.

**Keywords**: Interfacial chemistry, peroxy radicals, organic hydroperoxides, hydrogen-deuterium exchange, mass spectrometry

**Synopsis**: Hydroperoxyl radicals leads to the formation of organic hydroperoxides at aerosol particle interface during heterogeneous oxidation of organic aerosols in the atmosphere.

31 **TOC**:

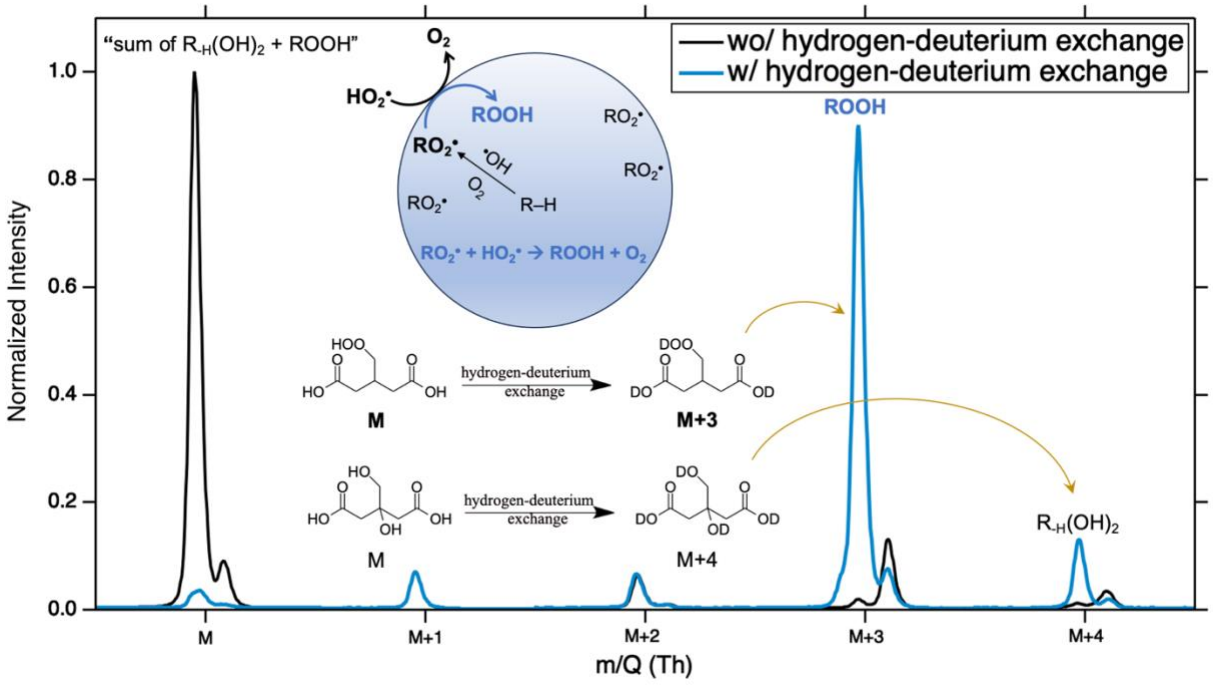
"sum of R-H(OH)2 + ROOH"
wo/ hydrogen-deuterium exchange
w/ hydrogen-deuterium exchange
Normalized Intensity
m/Q (Th)
M
M+1
M+2
M+3
M+4
ROOH
R-H(OH)2
HO2•
O2
RO2•
•OH
R–H
RO2• + HO2• → ROOH + O2
hydrogen-deuterium exchange
M
M+3
M+4

32

## Introduction

Organic aerosols (OA) account for a large fraction of fine particulate matter ($PM_{2.5}$) in the atmosphere, significantly impacting climate, visibility and human health.[1-3] Throughout their lifetime, OA particles undergo heterogeneous oxidative aging by gaseous oxidants, such as hydroxyl radical ($^{\bullet}OH$), which continuously affect their reactivity, chemical composition, and properties.[4-6] Hydroperoxyl radicals ($HO_2^{\bullet}$), closely coupled with $^{\bullet}OH$, are another important gas-phase reactive oxidants in the atmosphere and are primarily generated by daytime photochemical reactions.[7-9] The typical tropospheric $[HO_2^{\bullet}]/[^{\bullet}OH]$ ratios are approximately within the range of 10–100, with $[HO_2^{\bullet}]$ up to the order of $10^8$ molecules $cm^{-3}$.[10-13]

The oxidation mechanism and related kinetics of $HO_x^{\bullet}$ ($\equiv HO_2^{\bullet} + {}^{\bullet}OH$) reactions are well-studied in the gas phase.[14-17] $^{\bullet}OH$ initiates the oxidation of a generic gas-phase organic molecule (R–H) by H abstraction to produce an alkyl radical ($R^{\bullet}$), and a subsequent peroxy radical ($RO_2^{\bullet}$) is formed after molecular oxygen addition. In the absence of nitrogen oxides, the $RO_2^{\bullet}$ primarily undergo bimolecular reactions with $HO_2^{\bullet}$ to form organic hydroperoxides (ROOH) and with another $RO_2^{\bullet}$ to produce an alcohol-carbonyl pair (i.e., ROH and $R_{-H}{=}O$), wherein both pathways could also form alkoxy radicals ($RO^{\bullet}$) with varied branching ratios depending on the $RO_2^{\bullet}$ structure.[18-23] The labile hydroperoxide functionality in ROOH has a significant impact on the subsequent organic degradation and evolution in both the gas and particle phases.[19, 24-26] In strong contrast to this well-known gas-phase $HO_2^{\bullet}$ chemistry, the mechanistic understanding of the multiphase $HO_2^{\bullet}$ processes is very limited despite that kinetic observations of $HO_2^{\bullet}$ uptake on the interface of aerosol particles have been widely reported, especially for aqueous aerosols.[27-32] For example, Lakey et al.[29] reported $HO_2^{\bullet}$ uptake onto aerosol particles with the uptake coefficient from $< 0.004$ (dry particles) to ~0.09 (aqueous particles) in laboratory studies; Copper et al.[27] and

Zhou et al.[31] observed $HO_2^•$ uptake onto ambient aerosols with the uptake coefficient of 0.025 – 0.24. George and Abbatt[6] summarized the heterogeneous $^•OH$ oxidation mechanisms of OA in analogy to the gas-phase oxidation and proposed that the $RO_2^•$ + $HO_2^•$ reactions proceed in a similar manner leading to ROOH formation. But to our knowledge, no prior work has reported the direct observation of this pathway. For instance, previous studies have attempted to indirectly probe ROOH formation by including the reaction mechanism in a kinetic model[23] or estimating the number of oxygen atoms added per reacted parent OA.[33] But conclusive evidence for ROOH formation in heterogeneous oxidation was not provided due to the challenges in directly detecting ROOH. Furthermore, it is unclear how gaseous $HO_2^•$ affects heterogeneous OA oxidation kinetics and molecular composition by regulating $RO^•$ formation and hence secondary chain propagation chemistry.[6, 23, 34] Lastly, it is also elusive whether the $RO_2^•$ + $HO_2^•$ reactions (if any) occur at the particle interface following collisions or in the bulk by the absorption mechanism.[29]

In the study, we perform $^•OH$-initiated heterogeneous oxidation experiments of several oxygenated OA model systems under varied [$^•OH$] and [$HO_2^•$] with controlled [$HO_2^•$]/[$^•OH$] ratios. These OA model surrogates contain multiple functional groups with a wide range of O/C ratios of 0.40 – 1.00, representing moderately to highly oxidized OA in the atmosphere. We characterize the molecular composition of the heterogeneously oxidized OA by a suite of mass spectrometry instrumentation.[5, 35-37] From these measurements, we report direct observation of ROOH formation and propose the $^•OH$-initiated heterogeneous OA oxidation mechanisms under atmospherically relevant [$HO_2^•$]/[$^•OH$] ratios.

## Materials and Methods

### *Chemicals and reagents*

The chemicals and reagents with their purities and suppliers used in this study are as follows: 3-methylglutaric acid (TCI, >99.0%), adipic acid (Sigma-Aldrich, ≥99.5%), glucose (TCI, >98%), tricarballylic acid (Acros Organics, 99%), 1, 2, 3, 4-butanetetracarboxylic acid (Acros Organics, >99%), camphoric acid (Sigma-Aldrich, 99%), 1, 3, 5-cyclohexanetricarboxylic acid (Sigma-Aldrich, cis 90%), suberic acid (TCI, >99%), xylitol (Acros Organics, >99%), methanol (Fisher Chemical, 99.9%), hydrogen peroxide ($H_2O_2$, Fisher Chemical, 30% aq. soln.), water (Fisher Chemical, HPLC Grade Submicron Filtered), deuterium oxide (thermo scientific, 99.8 atom % D), toluene (Certified ACS, 99.9%), pyridine (DriSolv., 99.8%), BSTFA W/1% TMCS (Restek Corporation), acetonitrile (Fisher Chemical, 99.95%), tartaric acid (TCI, >99.0%) and isoprene (Alfa Aesar, 99%). None of the above chemicals nor regents were used with further purification.

### *Experimental details*

All experiments were carried out in a Quartz laminar flow tube reactor (FTR, ~4.12 L) under room temperature (~ 295 ± 2 K).[5, 35-39] The relative humidity (RH) was adjusted by controlling the fractions of clean dry air through vs. bypassing a water bubbler to achieve the relatively high-RH condition (77 ± 3%) or low-RH condition (32 ± 3%). The total flow rate in the FTR was 4 L $min^{-1}$, corresponding to a residence time of ~ 60 s. $O_3$ was introduced into the FTR by passing pure $O_2$ through an ozone generator (Jelight, Model 610). $^{\bullet}OH$ were generated by $O_3$ photolysis in the presence of water vapor by two mercury UV lamps ($\lambda$ = 254 nm). A total of nine OA model compounds with multiple different functional groups were studied under high-RH

conditions, including 3-methylglutaric acid ($C_6H_{10}O_4$), adipic acid ($C_6H_{10}O_4$), glucose ($C_6H_{12}O_6$), tricarballylic acid ($C_6H_8O_6$), 1, 2, 3, 4-butanetetracarboxylic acid ($C_8H_{10}O_8$), camphoric acid ($C_{10}H_{16}O_4$), 1, 3, 5-cyclohexanetricarboxylic acid ($C_9H_{12}O_6$), suberic acid ($C_8H_{14}O_4$), and xylitol ($C_5H_{12}O_5$). A constant output aerosol atomizer (TSI Inc. Model 3076) was used to generate polydisperse OA particles from aqueous solutions (1 g $L^{-1}$) of these model compounds. The typical OA particle mass loading in the FTR was 2600 – 5000 μg $m^{-3}$; the mean surface-weighted particle diameters of the generated OA surrogates were in the range of 200 ± 20 nm – 240 ± 30 nm. The high aerosol mass loadings are necessary to ensure that minimal fractions of the OA species, which already have low volatilities, are in the gas phase such that any observed ROOH is formed in the condensed phase. For these nine model systems, two oxidation conditions were examined, i.e., $[HO_2^\bullet]/[^\bullet OH] < 1$ vs. $[HO_2^\bullet]/[^\bullet OH] \sim 40$ (see the section below and **Supporting Information, SI, Table S1** for experimental details). Among these OA surrogates, 3-methylglutaric acid was investigated in greater detail under more experimental conditions, including varied RH and particle sizes, more scattered $[HO_2^\bullet]/[^\bullet OH]$ scenarios, and more comprehensive product characterization. This allows for a closer examination of the $HO_2^\bullet$ heterogeneous chemistry and its impacts on the oxidation kinetics and OA molecular composition.

The OA particle size distribution and number concentration were measured by a scanning electrical mobility sizer (SEMS) and mixing condensation particle counter (MCPC), respectively (Brechtel Inc., 2100). $O_3$ concentration was measured by an ozone analyzer (Thermo Environmental Instrument, Inc., 49C) after a HEPA filter that removes particles at the FTR exit. The OA particles were guided through a charcoal denuder to remove gas-phase compounds followed by a 1.6 L $min^{-1}$ dilution flow containing humidified air with $H_2O$ or $D_2O$. With $D_2O$, it allows for hydrogen-deuterium exchange (HDX) on any labile hydrogen atoms (i.e., H in –O–H

and –O–O–H converted to D).[40] HDX is a useful approach to determine the number of active hydrogen attached to heteroatom, helping separate and detect individual molecules of alcohols, phenols, carboxylic acids, hydroperoxides, amines, and amides, etc. from complex mixtures.[41-43] However, the exchange of hydrogen and deuterium is reversible and the exchange rate relies on experimental conditions.[42, 43] Thus, the completeness of HDX needs to be verified. The diluted OA particles were then sampled by a thermal desorption chemical ionization time-of-flight mass spectrometer (TD-CIMS, Aerodyne Research Inc., m/Δm ~ 4000) with the $I^-$ chemical ionization source for real-time molecular composition analysis, with the TD temperature set to 180 °C to vaporize most OA species.[5, 38] The effectiveness of the set TD temperature was tested by measuring the ratios of particle mass loading through the TD tubing with versus without heating. As a result, under this TD temperature, only ~0.8% and ~1.6% of unoxidized and oxidized 3-methylglutaric acid particles remained in the particle phase, respectively, indicating the high efficiencies of vaporizing the OA particles into the gas phase. In addition to real-time characterization, aerosol samples at all oxidation stages were collected by a sequential spot sampler (Aerosol Devices Inc., SS110) for offline analyses using an electrospray ionization time-of-flight mass spectrometer in the negative ion mode ((–)ESI-MS, Aerodyne Research Inc.)[38] and a gas chromatography mass spectrometer (GC-MS, Agilent Inc., 7890 GC and 5975 MSD) with prior derivatization[39, 44, 45] in the 3-methylglutaric acid experiments. The (–)ESI-MS was utilized to examine the role of $HO_2^\bullet$ in the comprehensive OA molecular composition. The GC-MS analysis was conducted to study the $HO_2^\bullet$ impacts on heterogeneous OA oxidation kinetics and provide some insights into the isomer-resolved products.

***$HO_x^\bullet$ control and estimation***

For the heterogeneous oxidation experiments requiring higher [$HO_2^•$]/[$^•OH$], methanol was continuously injected into the FTR by a syringe pump (Chemyx Inc.) at controlled rates. The $^•OH$ oxidation of methanol is known to efficiently generate $HO_2^•$.[46-48] Without a detection method to directly quantify [$^•OH$] and [$HO_2^•$], their concentrations were estimated by a photochemical box model based on MCM v3.2 including all the inorganic gas-phase reactions and methanol oxidation mechanism.[39, 49, 50] The chemical reactions to generate $^•OH$ and $HO_2^•$ in the box model are listed in the **SI**, **Table S2**. The estimation of [$^•OH$] was carried out using this approach in our prior studies.[39, 51] In these reactions, the only unknown parameters are $O_3$ photolysis rate constant and $^•OH$ and $HO_2^•$ wall loss rate constants.[51] We set these values as tuning parameters and optimized their values to reach the best measurement-simulation agreement. Specifically, the measured and simulated [$O_3$] were used to constrain $O_3$ photolysis rates; [$^•OH$] experimentally determined by the consumption of methanol measured using a high-sensitivity proton-transfer-reaction mass spectrometer (PTR-MS, Ionicon Analytik Inc.) were used to constrain $^•OH$ wall loss rate constant in the box model. Lastly, the production of $H_2O_2$ has been used to estimate [$HO_2^•$] in prior research because $HO_2^•$ is the principal $H_2O_2$ source.[52, 53] We followed the same approach and constrained the $HO_2^•$ wall loss rate constant by comparing simulated [$H_2O_2$][53] with that quantified using $H_2O_2$ standards detected by $I^-$-CIMS. The model performance was verified by comparing simulation outputs and measurements in characteristic experiments (**Figure S1**). The comparison results suggest that the model can simulate [$^•OH$] and [$HO_2^•$] within 30% accuracy under most experimental conditions. The model results suggest that in the absence of added methanol, $HO_2^•$ can be produced by $^•OH + O_3$, but the resultant [$HO_2^•$]/[$^•OH$] ratio is only < 1, much lower than atmospheric conditions. With methanol oxidized by $^•OH$, we can achieve much higher

168 [$HO_2^•$]/[$^•OH$] by regulating $O_3$ and methanol injection concentrations. We hence used this box
169 model to design the initial [$O_3$] and [methanol] in experiments to reach controllable [$HO_2^•$]/[$^•OH$]
170 with maximum values ~ 55, which is relevant to real atmospheric conditions. The $^•OH$ exposure
171 ranged from $9 \times 10^{10}$ to $4 \times 10^{12}$ molecules $cm^{-3}$ s in all experiments.
172
173 **Results and Discussion**
174 ***ROOH formation during OA heterogeneous oxidation***
175 Consistent with the well-accepted mechanism described above, the OH-initiated
176 heterogeneous oxidation of all the studied oxygenated OA surrogates forms a series of multi-
177 functionalized products through $RO_2^•$ self-reaction, including the first-generation products of
178 carbonyls ($R_{-H}=O$), alcohols (ROH), along with the second-generation products of dicarbonyls [$R_{-3H}(=O)_2$], hydroxycarbonyls [$R_{-2H}(=O)OH$], and diols [$R_{-H}(OH)_2$].[5, 6, 33, 35] Because ROOH and the
180 diol are isomers, it is impossible to differentiate them by typical mass spectrometry analysis,
181 causing challenges for ROOH identification. But because they are formed by different oxidation
182 generations and pathways, we attempt to demonstrate their different abundances under varied [$^•OH$]
183 and [$HO_2^•$]. In the (–)ESI-MS results for 3-methylglutaric acid oxidation shown in **Figure 1A**,
184 $C_6H_{10}O_6$ [sum of ROOH and $R_{-H}(OH)_2$] were formed with very limited fraction among all the
185 major functionalization products (< 1% signals) under [$HO_2^•$]/[$^•OH$] < 1 and low [$^•OH$]. Its relative
186 abundance increases with enhanced $^•OH$ exposure, indicative of the formation of the second-
187 generation product $R_{-H}(OH)_2$.[33] In contrast, under identical [$^•OH$] and thus likely similar amount
188 of $R_{-H}(OH)_2$, the fractions of $C_6H_{10}O_6$ are much greater (up to ~ 10%) with higher [$HO_2^•$]/[$^•OH$].
189 The gap is especially significant under lower [$^•OH$], suggesting that ROOH formed from $RO_2^•$ +
190 $HO_2^•$ is likely the dominant contributor to $C_6H_{10}O_6$ where multigenerational oxidation is limited.

Likewise, results from the TD-CIMS measurements of relative $C_6H_{10}O_6$ signals from 3-methylglutaric acid oxidation (**Figure 1B**) under two constant conditions of •OH exposure conditions both exhibit increasing trends as a function of [$HO_2$•], supporting formation of ROOH from $RO_2$• + $HO_2$•. Notably, the fractions of $C_6H_{10}O_6$ among the major products are always higher under lower •OH exposure condition, further suggesting that ROOH as a main contributor.

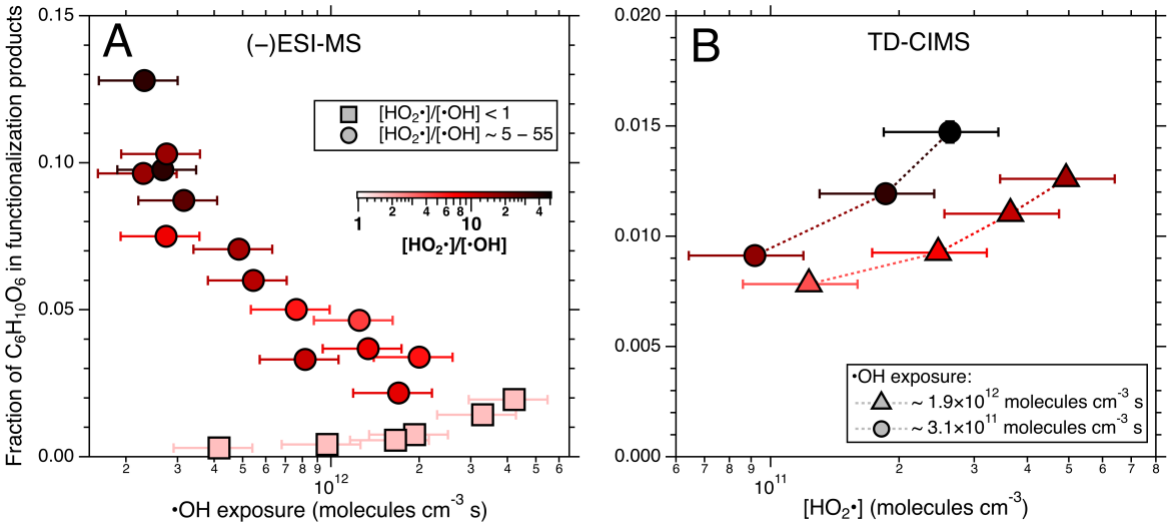


**Figure 1.** The fractions of $C_6H_{10}O_6$ in all the functionalization products, including $C_6H_8O_5$ ($R\text{-}_H{=}O$), $C_6H_{10}O_5$ (ROH), $C_6H_6O_6$ [$R\text{-}_{3H}(=O)_2$], $C_6H_8O_6$ [$R\text{-}_{2H}(=O)OH$], and $C_6H_{10}O_6$ [sum of ROOH and $R\text{-}_H(OH)_2$], from 3-methylglutaric acid oxidation in (A) (–)ESI-MS results as a function of •OH exposure; and (B) TD-CIMS results as a function of [$HO_2$•]. The [$HO_2$•]/[•OH] ratios ranged between < 1 and 55 are indicated by the color scheme shown in (A).

**Figure 2** illustrates the TD-CIMS mass spectra for the heterogeneously oxidized 3-methylglutaric acid and **Figures S3–S10** show similar results for the other studied OA surrogates. Two conditions with identical •OH exposure but very different [$HO_2$•]/[•OH] are focused with the ratio of < 1 (without methanol) and ~ 40 (with methanol, determined by the box model). The

$C_6H_{10}O_6$ signals in **Figures 2A–2B** show the sum of ROOH and $R\text{-}H(OH)_2$, which are much stronger with higher $[HO_2^\bullet]/[^\bullet OH]$ under similar $[^\bullet OH]$, while the differences for the other major peaks are negligible (**Figure 2B** vs. **2A**), indicating the enhanced ROOH formation from $RO_2^\bullet + HO_2^\bullet$ and agreeing with results illustrated in **Figure 1**. To unambiguously determine ROOH formation and abundance, we applied the HDX method to couple with the TD-CIMS to separate ROOH from $R\text{-}H(OH)_2$. HDX is expected to occur on functional groups with labile H atoms (i.e., H in –O–H and –O–O–H).[54-56] In the experiments using $D_2O$, the $I^-$ clusters of a detectable organic molecule (i.e., $[M+I]^-$) were observed to undergo a m/Q shift by mass units corresponding to the number of labile H atoms in the organic molecule structure. Under the assumption of identical sensitivity of ROOH and $R\text{-}H(OH)_2$ in TD-CIMS, the $I^-$ adduct ion of $C_6H_{10}O_6$ from 3-methylglutaric acid heterogeneous oxidation has a m/Q shift of 3 Th by ~85% based on peak intensities, corresponding to the ROOH, and a m/Q shift of 4 Th by ~15%, corresponding to the $R\text{-}H(OH)_2$ (**Figure 2C**). This directly demonstrates that ROOH is the major form of $C_6H_{10}O_6$ under the studied conditions. We ruled out the possibility of incomplete HDX for $R\text{-}H(OH)_2$ by testing tartaric acid, a chemical with two carboxylic acid groups and two alcohol groups, which exhibits complete HDX with a m/Q shift of 4 Th (**Figure S2**). The other studied OA model compounds with multiple alcohols or carboxylic acids also exhibit complete HDX. These results elucidate the formation of ROOH during heterogeneous $^\bullet OH$ oxidation of OA for the first time. In a prior work, ROOH formation has also been reported during $^\bullet OH$ oxidation of electrospray-generated microdroplets, but whether its formation was from gaseous $HO_2^\bullet$ reacting with aqueous $RO_2^\bullet$ at the microdroplet interface was not fully examined.[57] As a minor note, the m/Q shifts for the other species in the mass spectra are also consistent with their expected functionalities. As shown in **Figure 2C**, most of the initial $C_6H_{10}O_6$ signals are contributed by ROOH under atmospherically

relevant [$HO_2^•$]/[$^•$OH], strongly supporting the importance of ROOH from $RO_2^•$ + $HO_2^•$ during heterogeneous $^•$OH oxidation.

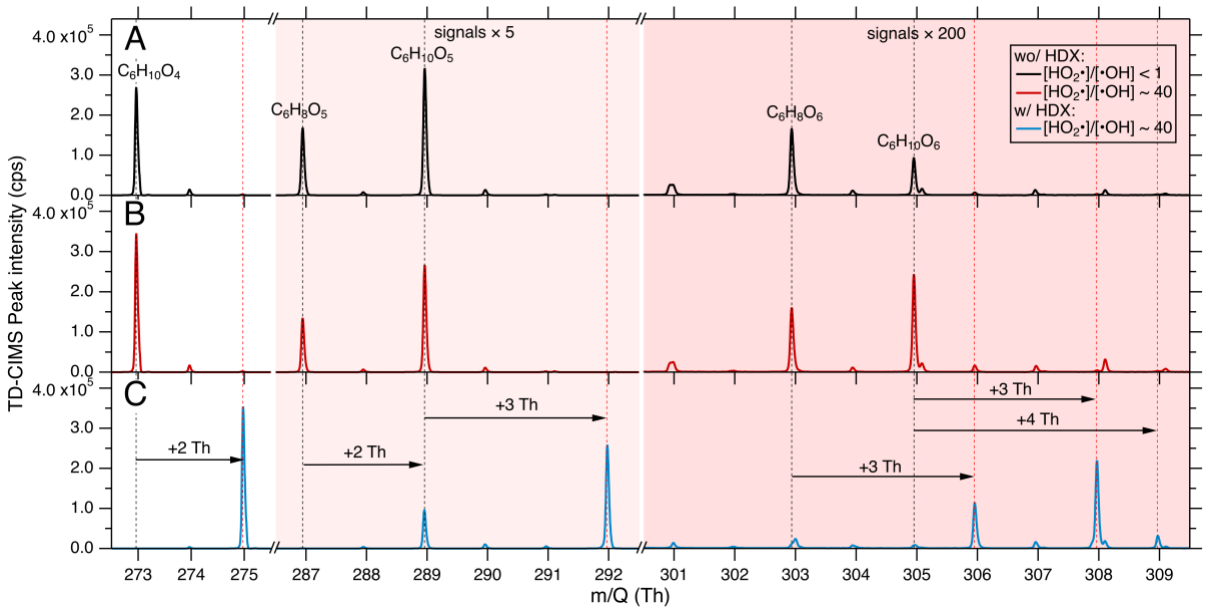


**Figure 2.** The mass spectra of $^•$OH-initiated heterogeneous oxidation of 3-methylglutaric acid under (A) [$HO_2^•$]/[$^•$OH] < 1 in the presence of $H_2O$, (B) [$HO_2^•$]/[$^•$OH] ~ 40 in the presence of $H_2O$ and (C) [$HO_2^•$]/[$^•$OH] ~ 40 in the presence of $D_2O$. The major products are labeled with the mass spectra peaks and the mass shifts during HDX are indicated.

The unambiguous formation of ROOH was not only observed from the 3-methylglutaric acid systems, but also from the other studied OA surrogates, as shown in **Figures S3–S10**. We further calculated the intensity-based fractions of ROOH among the first-generation functionalization products (i.e., the sum of ROOH, $R_{-H}$=O, and ROH) in the oxidized OA under a range of $^•$OH exposure ($7.6 \times 10^{11}$–$1.5 \times 10^{12}$ molecules $cm^{-3}$ s) for all the investigated OA surrogates (**Figure 3**). We found that high [$HO_2^•$]/[$^•$OH] leads to an increase in the ROOH fractions for all the model systems except for tricarballylic acid. This suggests that the proposed ROOH

formation from $RO_2^\bullet + HO_2^\bullet$ is rather a generic reaction during heterogeneous oxidation of OA. The relative abundance of ROOH for these OA surrogates ranges from 0.37±0.02% to 10.37±1.10% under $[HO_2^\bullet]/[^\bullet OH] < 1$ but are enhanced to 1.83±0.06% − 24.95±0.53% under $[HO_2^\bullet]/[^\bullet OH] \sim 40$. It should also be emphasized that ROOH are known to be thermally labile and could undergo decomposition during thermal desorption in TD-CIMS.[58-61] To provide some quantitative constraint of the thermal decomposition, we generated a well-known gas-phase ROOH, isoprene hydroxy hydroperoxide (ISOPOOH, $C_5H_{10}O_3$)[53, 62-65] in the FTR from isoprene oxidation, which is the dominant product detected at m/Q 245 Th by $I^-$-CIMS.[66] The isoprene oxidation products including ISOPOOH was sampled by the TD-CIMS under room temperature and 180 °C (the same operation temperature for the oxidized OA model systems). We found that the $C_5H_{10}O_3$ signal dropped by ~2/3 under 180 °C (**Figure S11**), indicating that the actual ROOH can be 3 times more substantial than the results reported in **Figure 3**. Taking the ROOH thermal decomposition loss into account, the ROOH relative abundance in 3-methylglutaric acid heterogeneous oxidation under $[HO_2^\bullet]/[^\bullet OH] \sim 40$ are in similar magnitude between the TD-CIMS measurements (~6%) and the (−)ESI-MS data (~10%, **Figure 1**). The ROOH relative abundance among the first-generation functionalization products approximately reflects the branching ratio of $RO_2^\bullet + HO_2^\bullet$ against $RO_2^\bullet + RO_2^\bullet$. These results thus suggest that the branching ratio of $RO_2^\bullet + HO_2^\bullet$ in heterogeneous OA oxidation under atmospheric $[HO_2^\bullet]/[^\bullet OH]$ may account for up to ~50% of the $RO_2^\bullet$ bimolecular fates, estimated using the highest ROOH contribution shown in **Figure 3** considering thermal decomposition. We should note that this approximation assumes that all the functionalization products have similar sensitivities in $I^-$-CIMS and similar sensitivities in (−)ESI-MS, which is not confirmed due to the lack of authentic standards. But it is likely a reasonable estimate considering the similar chemical structures of the products for each OA surrogate system.

However, different ROOH may have distinct thermal decomposition behavior and treating all ROOH the same could lead to some uncertainties.

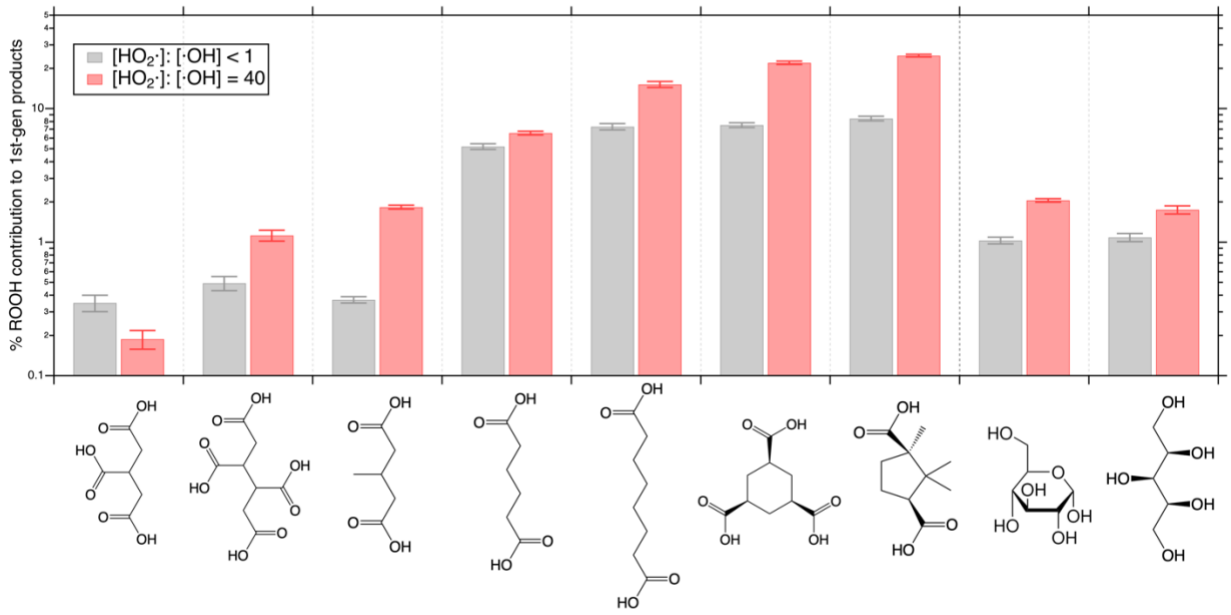


**Figure 3.** The intensity-based relative abundance (%) of ROOH among the first-generation oxidation products for different OA surrogates under $[HO_2^\bullet]/[^\bullet OH] < 1$ vs. $[HO_2^\bullet]/[^\bullet OH] \sim 40$.

Obviously, the ROOH enhancement (by a factor of 1.3 – 5.0) is to a much lesser degree compared to that of $[HO_2^\bullet]$ (by a factor of > 40) and the reason for this is unclear. We suspect that the $HO_2^\bullet$ uptake and reaction with $RO_2^\bullet$ is more efficient under lower $[HO_2^\bullet]$. The other possible explanation is that the bimolecular autoxidation (i.e., $RO_2^\bullet$ + R−H) that we previously proposed may partly contribute to the observed ROOH.[5] This would be surprising and may suggest that the bimolecular autoxidation may be rapid enough to compete with $RO_2^\bullet$ + $RO_2^\bullet$/ $HO_2^\bullet$ reactions even under high $[^\bullet OH]$. Future studies are warranted to elucidate the ROOH formation mechanisms under low $[HO_2^\bullet]/[^\bullet OH]$. But regardless, the enhanced ROOH formation with higher $[HO_2^\bullet]/[^\bullet OH]$

reported here clearly demonstrates the occurrence and importance of $RO_2^\bullet$ + $HO_2^\bullet$ reactions in heterogeneous OA oxidation.

***The role of $HO_2^\bullet$ in heterogeneous oxidation kinetics and molecular composition***

With the elucidation of ROOH formation from $RO_2^\bullet$ + $HO_2^\bullet$ reactions, we continue to examine how $HO_2^\bullet$ affects the OA oxidative aging kinetics. It is well known that the $RO_2^\bullet$ + $RO_2^\bullet$ reactions may partly form $RO^\bullet$, which can abstract H from R–H and form $RO_2^\bullet$ (known as chain propagation). This process effectively contributes to the R–H degradation.[6, 34] The substantial presence of $HO_2^\bullet$ could compete with $RO_2^\bullet$ to react with $RO_2^\bullet$ and hence reduce the $RO^\bullet$ formation from $RO_2^\bullet$ + $RO_2^\bullet$ as a smaller fraction of $RO_2^\bullet$ undergoes self-reaction. By this mechanism, it is expected that the OA oxidation kinetics may be slower with enhanced $HO_2^\bullet$. Here, we investigated the degradation of 3-methylglutaric acid as a function of $^\bullet$OH exposure and obtained the oxidation kinetics from the GC-MS measurements. As shown in **Figure S12**, the enhancement of $HO_2^\bullet$ plays a negligible role in the decay rates of 3-methylglutaric acid within the measurement uncertainties, suggesting that the $RO_2^\bullet$ + $HO_2^\bullet$ reactions offset the reduced $RO^\bullet$ formation from inhibited $RO_2^\bullet$ + $RO_2^\bullet$ and sustain the secondary chemistry. This can be explained by that $RO_2^\bullet$ + $HO_2^\bullet$ reactions also directly produce $RO^\bullet$ (and release $^\bullet$OH);[20-23] the ROOH may also be photolyzed into $RO^\bullet$ and $^\bullet$OH.[19, 23-26] Indicated by the kinetic results for the case of 3-methylglutaric acid, the $RO^\bullet$ and $^\bullet$OH from $RO_2^\bullet$ + $HO_2^\bullet$ contributed to 3-methylglutaric acid oxidation to a similar extent as $RO^\bullet$ from $RO_2^\bullet$ + $RO_2^\bullet$.

As reported by Kurtén et al.[67] for gas-phase $RO_2^\bullet$ + $HO_2^\bullet$, the $RO^\bullet$ + $^\bullet$OH formation pathway may have a large branching ratio if the $RO_2^\bullet$ is on a tertiary carbon.[21-23] In contrast, the

less substituted primary and secondary $RO_2^\bullet$ are likely the main contributors to ROOH formation. In the case of 3-methylglutaric acid, the primary oxidation site is the tertiary carbon, followed by the primary carbon, while the two secondary carbons adjacent to the carboxylic acids are less oxidized due to the mesomeric effect, as discussed in our prior work and supported by new isomer-resolved GC-MS results (**Figure S13**).[35] For example, the dominant alcohol product (> 80%) has the –OH group on the tertiary carbon; the dominant carbonyl product (> 80%) has the C=O group on the primary carbon (i.e., an aldehyde). This aldehyde tends to be further oxidized into tricarballylic acid. Based on this, a mechanism for 3-methylglutaric acid $^\bullet$OH oxidation is shown in **Figure 4**.[6, 23, 68, 69] It is expected that, by reacting with $HO_2^\bullet$, the dominant tertiary $RO_2^\bullet$ mainly produces $RO^\bullet$ + $^\bullet$OH and the less abundant primary $RO_2^\bullet$ mainly forms ROOH.[21-23] This agrees with that the relative abundance of ROOH during 3-methylglutaric acid oxidation is on the lower side among all the studies OA surrogates (**Figure 3**). In fact, as shown in **Figure 3**, all the studied OA model compounds with tertiary carbons as the primary oxidation sites have relatively lower ROOH abundance, while those with secondary and primary carbons as the main oxidation sites (i.e., 1, 3, 5-cyclohexanetricarboxylic acid, camphoric acid, adipic acid and suberic acid) exhibit much stronger ROOH formation. These discrepancies among different OA model systems are highly consistent with our proposed $RO_2^\bullet$ + $HO_2^\bullet$ mechanisms.

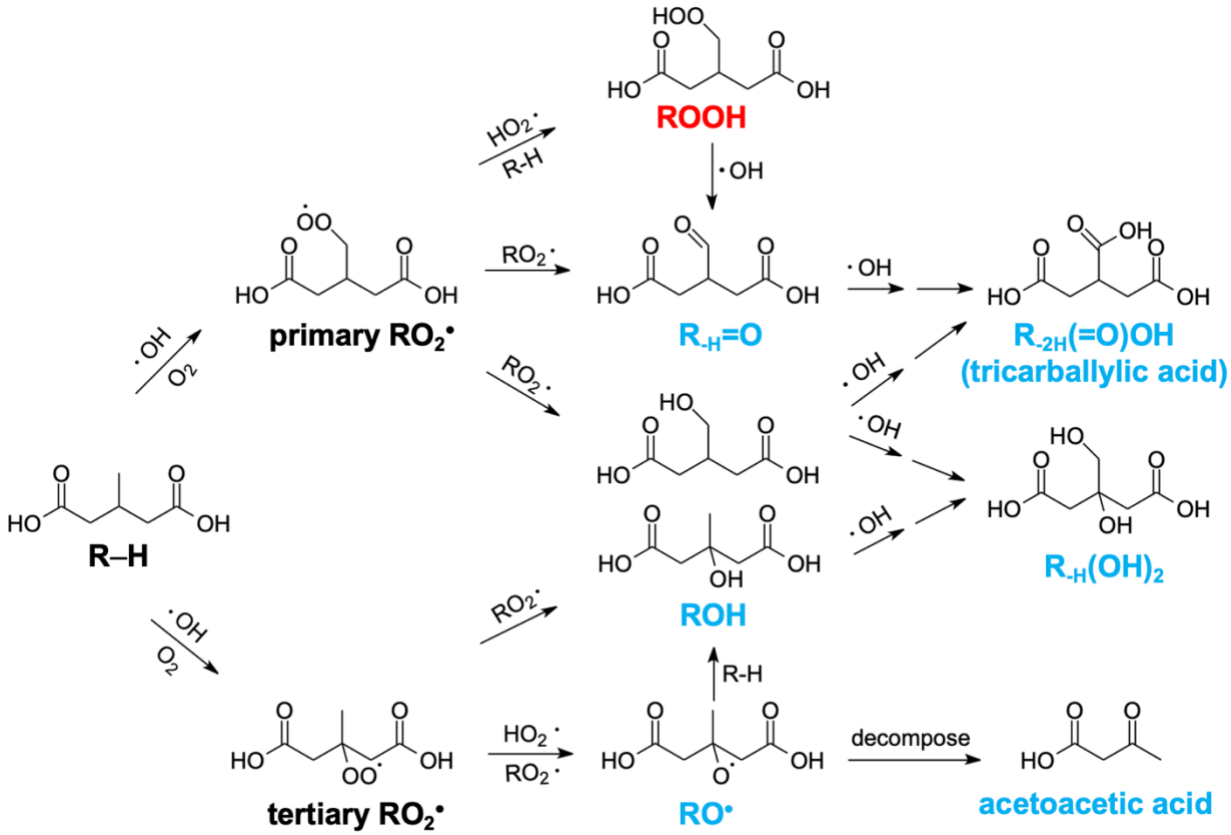


321

322 **Figure 4.** The proposed mechanism of •OH-initiated heterogeneous oxidation of 3-methylglutaric

323 acid mediated by $HO_2$• reactions.

324

325 Despite the little influence on the oxidation kinetics for 3-methylglutaric acid, $HO_2$• have

326 a greater impact on OA molecular composition through heterogeneous oxidation. As expected, the

327 formation of ROH and $R_{-H}$=O from $RO_2$• + $RO_2$• reactions is suppressed under high [$HO_2$•]/[•OH]

328 because more $RO_2$• react with $HO_2$• (**Figure S14A – B**). Due to the RO• produced from $RO_2$• +

329 $HO_2$• sustaining the chain propagation chemistry from which ROH is a product (**Figure 4**),[20-23] it

330 is also expected that suppression for ROH is to a lesser extent than $R_{-H}$=O. However, this is not

331 the case. In fact, the ratio of $R_{-H}$=O/ROH slightly increases with higher $HO_2$• (**Figure S15**),

332 indicating an efficient pathway to form $R_{-H}$=O with ROOH involved. We suggest that $R_{-H}$=O can

be formed from further •OH oxidation of the primary ROOH with •OH as the co-product (**Figure 4**). The tertiary RO• can also undergo fragmentation reactions to produce smaller molecules, mainly acetoacetic acid ($C_4H_6O_3$, **Figure 4**).[5, 34] As shown in **Figure S16A**, the absolute intensities of acetoacetic acid measured by TD-CIMS under different [$HO_2$•]/[•OH] vary insignificantly, agreeing with the discussion above that $RO_2$• + $HO_2$• reactions offset the decreased formation of RO• from $RO_2$• + $RO_2$•. On the other hand, the much higher abundance of acetoacetic acid relative to ROH + $R_{-H}$=O in the presence of additional $HO_2$• (**Figure S16B**) suggests that a great fraction of the RO• that undergoes fragmentation comes from $RO_2$• + $HO_2$•, rather than $RO_2$• + $RO_2$•.

Finally, we examined how $HO_2$• affected the overall OA composition. As shown in **Figure S17,** we present the average carbon oxidation state ($OS_C$) and O/C ratio from the 3-methylglutaric acid heterogeneous oxidation under different [$HO_2$•] and [•OH] conditions, based on the observed (–)ESI-MS intensities of all the observed oxidation products with chemical formulas of $C_{1\text{-}6}H_{2\text{-}10}O_{3\text{-}8}$. The $OS_C$ and O/C ratios increase by ~0.10 and ~0.05, respectively, as [$HO_2$•] increased by sevenfold under a constant lower [•OH] of ~ $4.4 \times 10^9$ molecules $cm^{-3}$, indicating that $HO_2$• facilitates OA chemical evolution. In contrast, in similar experiments but with higher [•OH] of ~ $2.4 \times 10^{10}$ molecules $cm^{-3}$, the $OS_C$ and O/C ratios do not exhibit as prominent increasing trends with enhanced [$HO_2$•]. These results suggest that under high [•OH] and hence high [$RO_2$•], $RO_2$• + $RO_2$• reactions are already sufficient, and thus the impacts of $HO_2$• on the overall heterogeneous oxidative aging is less pronounced.

***The interfacial nature of $RO_2$• + $HO_2$•***

In order to further investigate where the $RO_2^\bullet + HO_2^\bullet$ reactions take place in the particles, we examined ROOH formation under both high-RH and low-RH conditions using 3-methylglutaric acid. It was expected that the $HO_2^\bullet$ uptake is more effective under higher RH,[28, 30] but surprisingly, the ROOH formation was higher under lower RH regardless of $[HO_2^\bullet]/[^\bullet OH]$ (**Figure 5A**). The higher ROOH relative abundance under the low-RH condition turns out to be a result of both more strongly increased ROOH signals and decreased $R_{-H}=O$ and ROH signals from the TD-CIMS measurements. The more prominent decrease in $R_{-H}=O$ and ROH intensities under lower RH is expected due to larger diffusion limitation and reduced parent OA reactivities.[70] But unexpectedly, the slower oxidation and hence reduced $RO_2^\bullet$ formation is somehow offset by the promoted $RO_2^\bullet + HO_2^\bullet$ which leads to higher ROOH. Previous studies have reported that aerosol particles containing low water contents tend to have negligible $HO_2^\bullet$ uptake due to the diffusion limitation.[28, 30] The key difference here is that the OA particles interacting with gaseous $HO_2^\bullet$ are oxidized and contain $RO_2^\bullet$ at the interface. We thus hypothesize that the higher ROOH fractions under lower RH is because the $RO_2^\bullet + HO_2^\bullet$ reaction takes place at the particle interface immediately after collision, rather than by the absorption mechanism. The viscosities for the probing compound, 3-methylglutaric acid, were estimated to be $2.06 \times 10^{1}$ and $6.22 \times 10^{-2}$ Pa s under low and high RH, respectively, using the AIOMFAC model as described in our previous work.[5, 39] Despite the reduced total $RO_2^\bullet$ formation under the low-RH conditions, the formed $RO_2^\bullet$ are less mobile and more effectively accumulated at the particle surface region due to slower diffusion, allowing the colliding $HO_2^\bullet$ to react with the interfacial $RO_2^\bullet$ more readily. Previous studies suggested that functionalized ROOH such as hydroxymethyl hydroperoxides[71] and α-acyloxyalkyl hydroperoxides[72] may undergo water-catalyzed decomposition, with the decomposition time scale for α-acyloxyalkyl hydroperoxides at ~10–30 min. This is much longer

than the experimental time scale in this work (i.e., ~1 min). For the generic ROOH studied here, the aqueous decomposition is likely even slower, which suggests that aqueous decomposition is not the major reason for our observation shown in **Figure 5A**. In addition, the oxidized aerosols under two different RH conditions were collected by the spot sampler where the particles were grown into aqueous droplets under supersaturation conditions and sit in the form of droplets for a few minutes before the (–)ESI-MS analysis. Thus, the fact that the (–)ESI-MS results (**Figure S18**) are consistent with those from TD-CIMS rules out possibility that the lower ROOH under the high-RH condition is due to aqueous decomposition. Rather, we suggest that the ROOH formation is indeed promoted under the low-RH condition. Moreover, by varying the concentration of 3-methylglutaric acid in the aerosol atomizer, the particle size distribution was also modified, resulting in varied particle surface-to-volume ratio by a factor of two. With increased surface-to-volume ratio, the ROOH relative abundance through the same heterogeneous oxidation experiments (i.e., identical [$^{\bullet}$OH] and [$HO_2^{\bullet}$]) also increased (**Figure 5B**), supporting the above hypothesis that the $RO_2^{\bullet}$ + $HO_2^{\bullet}$ reaction occurs at particle interface. In the atmosphere, particle surface uptake is an important loss pathway for gaseous $HO_2^{\bullet}$.[27, 31, 73] We suggest that the presence of $RO_2^{\bullet}$ at the interface in the particle bound could enhance the $HO_2^{\bullet}$ uptake and also heterogeneous ROOH formation.

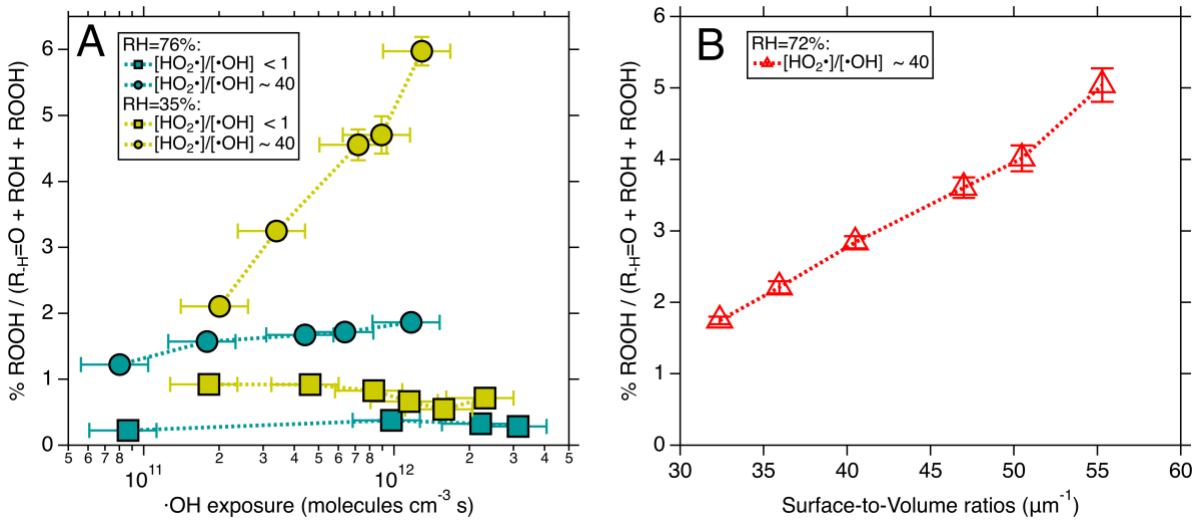


**Figure 5.** The fractions of ROOH among the first-generation functionalization products under (A) varied RH and $[HO_2^\bullet]/[^\bullet OH]$ conditions as a function of $^\bullet OH$ exposure, and (B) varied surface-to-volume ratios.

## Atmospheric Implications

In this work, we report heterogeneous $RO_2^\bullet + HO_2^\bullet$ reactions during $^\bullet OH$-initiated oxidative aging for several oxygenated OA model systems. Direct observations of ROOH formation from these reactions are shown for the first time by using HDX with the TD-CIMS analysis. The heterogeneously formed ROOH may contribute significantly to the total oxidized OA. Evidence is also shown to support that the heterogeneous $RO_2^\bullet + HO_2^\bullet$ reactions may also produce $RO^\bullet + {}^\bullet OH$ for tertiary $RO_2^\bullet$, similar to that reported in the gas-phase systems.[20-23] These two $RO_2^\bullet + HO_2^\bullet$ reaction pathways together facilitate compositional change of the heterogeneously oxidized OA particles. This $HO_2^\bullet$-involved chemistry is suggested to occur at the particle interface and is promoted when the interface is enriched with $RO_2^\bullet$.

Prior field observations suggested significant loss of $HO_2^\bullet$ through aerosol uptake.[74-77] The work reported here provides new mechanistic insights into the subsequent fates of the uptaken $HO_2^\bullet$ in the particle phase. The first $RO_2^\bullet + HO_2^\bullet$ pathway leads to the formation of ROOH, which are a class of reactive oxygen species that are known to cause adverse health effects.[78] This reaction has been highly emphasized in the gas phase for decades because ROOH substantially contribute to the atmospheric secondary organic aerosols.[18, 65, 79] The ROOH formation via heterogeneous oxidative reactions reported here has not been recognized despite of the general hypothesis.[6] The other $RO_2^\bullet + HO_2^\bullet$ pathway forms $RO^\bullet + {}^\bullet OH$,[20-23] thus recycling radicals in the condensed phase and propagating secondary chemistry. In the explicitly studied 3-methylglutaric acid system, this pathway is likely very important, owing to the tertiary carbon as the primary oxidation site. It remains to be studied to what extent the other OA model compounds undergo this pathway and how the varied results may affect the overall oxidation kinetics. It is likely that for compounds that more dominantly undergo the first pathway and form ROOH, the overall oxidation could be slower. Nevertheless, the products from heterogeneous $RO_2^\bullet + HO_2^\bullet$ reactions are crucial species and intermediates and may impact the OA composition and properties significantly.

This work, together with several of our prior studies,[5, 36, 39] demonstrate that the multiphase oxidation of OA particles can have very complex mechanisms and kinetics, especially when the oxidation occurs under atmospherically relevant conditions (e.g., in the presence of inorganic species, lower [$^\bullet$OH], and higher [$HO_2^\bullet$]/[$^\bullet$OH]). These results suggest that typical laboratory experiments do not accurately mimic atmospheric multiphase oxidation processes. The key environmental factors need to be better represented in laboratory setup and their influences need to be systematically investigated in future studies to help better understand OA chemical evolution in the atmosphere.

## Associated Contents

Supporting Information

Additional experimental details, MCM model simulations for $HO_x^{\bullet}$ estimation, additional mass spectra for chemical standards and oxidation products, GC-MS data, and supplementary kinetic and chemical composition results.

## Author Information

Corresponding Authors

E-mail address: haofei.zhang@ucr.edu (H. Zhang).

Notes

The authors declare no competing financial interest.

## Acknowledgements

This work is supported by the U.S. National Science Foundation (CHE-2002413). K. I. was supported by the Research in Science and Engineering (RISE) undergraduate research program at UC Riverside.

## References


(1) B oucher, O.; Randall, D.; Artaxo, P.; Bretherton, C.; Feingold, C.; Forster, P.; Kerminen, V.-M.; Kondo, Y.; Liao, H.; Lohmann, U.; et al. *Clouds and Aerosols*; IPCC: 2013; p 657.

(2) D ockery, D. W.; Pope, C. A.; Xu, X.; Spengler, J. D.; Ware, J. H.; Fay, M. E.; Ferris, B. G.; Speizer, F. E. An Association between Air Pollution and Mortality in Six U.S. Cities. *N. Engl. J. Med.* **1993**, *329* (24), 1753-1759.

(3) Ramanathan, V.; Crutzen, P. J.; Kiehl, J. T.; Rosenfeld, D. Aerosols, Climate, and the Hydrological Cycle. *Science* **2001**, *294* (5549), 2119-2124.

(4) Kristiansen, N. I.; Stohl, A.; Olivié, D. J. L.; Croft, B.; Søvde, O. A.; Klein, H.; Christoudias, T.; Kunkel, D.; Leadbetter, S. J.; Lee, Y. H.; et al. Evaluation of observed and modelled aerosol lifetimes using radioactive tracers of opportunity and an ensemble of 19 global models. *Atmos. Chem. Phys.* **2016**, *16* (5), 3525-3561.

(5) Zhang, W.; Zhao, Z.; Shen, C.; Zhang, H. Unexpectedly Efficient Aging of Organic Aerosols Mediated by Autoxidation. *Environ. Sci. Technol.* **2023**, *57* (17), 6965-6974.

(6) George, I. J.; Abbatt, J. P. D. Heterogeneous oxidation of atmospheric aerosol particles by gas-phase radicals. *Nat. Chem.* **2010**, *2* (9), 713-722.

(7) Calvert, J. G.; Pitts, J. N. *Photochemistry*; Wiley, 1966.

(8) González Palacios, L.; Corral Arroyo, P.; Aregahegn, K. Z.; Steimer, S. S.; Bartels-Rausch, T.; Nozière, B.; George, C.; Ammann, M.; Volkamer, R. Heterogeneous photochemistry of imidazole-2-carboxaldehyde: $HO_2$ radical formation and aerosol growth. *Atmos. Chem. Phys.* **2016**, *16* (18), 11823-11836.

(9) Stone, D.; Whalley, L. K.; Heard, D. E. Tropospheric OH and $HO_2$ radicals: field measurements and model comparisons. *Chem. Soc. Rev.* **2012**, *41* (19), 6348-6404.

(10) Fuchs, H.; Brauers, T.; Dorn, H. P.; Harder, H.; Häseler, R.; Hofzumahaus, A.; Holland, F.; Kanaya, Y.; Kajii, Y.; Kubistin, D.; et al. Technical Note: Formal blind intercomparison of $HO_2$ measurements in the atmosphere simulation chamber SAPHIR during the HOxComp campaign. *Atmos. Chem. Phys.* **2010**, *10* (24), 12233-12250.

(11) Nussbaumer, C. M.; Fischer, H.; Lelieveld, J.; Pozzer, A. What controls ozone sensitivity in the upper tropical troposphere? *EGUsphere* **2023**, *2023*, 1-25.

(12) Levy, H. Normal Atmosphere: Large Radical and Formaldehyde Concentrations Predicted. *Science* **1971**, *173* (3992), 141-143.

(13) McConnell, J. C.; McElroy, M. B.; Wofsy, S. C. Natural Sources of Atmospheric CO. *Nature* **1971**, *233* (5316), 187-188.

(14) Atkinson, R. Kinetics and mechanisms of the gas-phase reactions of the hydroxyl radical with organic compounds under atmospheric conditions. *Chem. Rev.* **1986**, *86* (1), 69-201.

(15) Atkinson, R.; Arey, J. Atmospheric Degradation of Volatile Organic Compounds. *Chem. Rev.* **2003**, *103* (12), 4605-4638.

(16) Orlando, J. J.; Tyndall, G. S. Laboratory studies of organic peroxy radical chemistry: an overview with emphasis on recent issues of atmospheric significance. *Chem. Soc. Rev.* **2012**, *41* (19), 6294-6317.

(17) Ziemann, P. J.; Atkinson, R. Kinetics, products, and mechanisms of secondary organic aerosol formation. *Chem. Soc. Rev.* **2012**, *41* (19), 6582-6605.

(18) Kroll, J. H.; Seinfeld, J. H. Chemistry of secondary organic aerosol: Formation and evolution of low-volatility organics in the atmosphere. *Atmos. Environ.* **2008**, *42* (16), 3593-3624.

(19) Docherty, K. S.; Wu, W.; Lim, Y. B.; Ziemann, P. J. Contributions of Organic Peroxides to Secondary Aerosol Formed from Reactions of Monoterpenes with $O_3$. *Environ. Sci. Technol.* **2005**, *39* (11), 4049-4059.
(20) D'Ambro, E. L.; Hyttinen, N.; Møller, K. H.; Iyer, S.; Otkjær, R. V.; Bell, D. M.; Liu, J.; Lopez-Hilfiker, F. D.; Schobesberger, S.; Shilling, J. E.; et al. Pathways to Highly Oxidized Products in the Δ3-Carene + OH System. *Environ. Sci. Technol.* **2022**, *56* (4), 2213-2224.
(21) Iyer, S.; Reiman, H.; Møller, K. H.; Rissanen, M. P.; Kjaergaard, H. G.; Kurtén, T. Computational Investigation of $RO_2$ + $HO_2$ and $RO_2$ + $RO_2$ Reactions of Monoterpene Derived First-Generation Peroxy Radicals Leading to Radical Recycling. *J. Phys. Chem. A* **2018**, *122* (49), 9542-9552.
(22) Hasson, A. S.; Tyndall, G. S.; Orlando, J. J.; Singh, S.; Hernandez, S. Q.; Campbell, S.; Ibarra, Y. Branching Ratios for the Reaction of Selected Carbonyl-Containing Peroxy Radicals with Hydroperoxy Radicals. *J. Phys. Chem. A* **2012**, *116* (24), 6264-6281.
(23) McNeill, V. F.; Yatavelli, R. L. N.; Thornton, J. A.; Stipe, C. B.; Landgrebe, O. Heterogeneous OH oxidation of palmitic acid in single component and internally mixed aerosol particles: vaporization and the role of particle phase. *Atmos. Chem. Phys.* **2008**, *8* (17), 5465-5476.
(24) Tong, H.; Arangio, A. M.; Lakey, P. S. J.; Berkemeier, T.; Liu, F.; Kampf, C. J.; Brune, W. H.; Pöschl, U.; Shiraiwa, M. Hydroxyl radicals from secondary organic aerosol decomposition in water. *Atmos. Chem. Phys.* **2016**, *16* (3), 1761-1771.
(25) Vereecken, L.; Müller, J. F.; Peeters, J. Low-volatility poly-oxygenates in the OH-initiated atmospheric oxidation of α-pinene: impact of non-traditional peroxyl radical chemistry. *Phys. Chem. Chem. Phys.* **2007**, *9* (38), 5241-5248.
(26) Epstein, S. A.; Blair, S. L.; Nizkorodov, S. A. Direct photolysis of α-pinene ozonolysis secondary organic aerosol: Effect on particle mass and peroxide content. *Environ. Sci. Technol.* **2014**, *48* (19), 11251-11258.
(27) Cooper, P. L.; Abbatt, J. P. D. Heterogeneous Interactions of OH and $HO_2$ Radicals with Surfaces Characteristic of Atmospheric Particulate Matter. *J. Phys. Chem.* **1996**, *100* (6), 2249-2254.
(28) Lakey, P. S. J.; Berkemeier, T.; Krapf, M.; Dommen, J.; Steimer, S. S.; Whalley, L. K.; Ingham, T.; Baeza-Romero, M. T.; Pöschl, U.; Shiraiwa, M.; et al. The effect of viscosity and diffusion on the $HO_2$ uptake by sucrose and secondary organic aerosol particles. *Atmos. Chem. Phys.* **2016**, *16* (20), 13035-13047.
(29) Lakey, P. S. J.; George, I. J.; Whalley, L. K.; Baeza-Romero, M. T.; Heard, D. E. Measurements of the $HO_2$ uptake coefficients onto single component organic aerosols. *Environ. Sci. Technol.* **2015**, *49* (8), 4878-4885.
(30) Thornton, J.; Abbatt, J. P. D. Measurements of HO2 uptake to aqueous aerosol: Mass accommodation coefficients and net reactive loss. *J. Geophys. Res.: Atmos.* **2005**, *110* (D8).
(31) Zhou, J.; Murano, K.; Kohno, N.; Sakamoto, Y.; Kajii, Y. Real-time quantification of the total $HO_2$ reactivity of ambient air and HO2 uptake kinetics onto ambient aerosols in Kyoto (Japan). *Atmos. Environ.* **2020**, *223*, 117189.
(32) Taketani, F.; Kanaya, Y.; Akimoto, H. Heterogeneous loss of HO2 by KCl, synthetic sea salt, and natural seawater aerosol particles. *Atmos. Environ.* **2009**, *43* (9), 1660-1665.
(33) Smith, J. D.; Kroll, J. H.; Cappa, C. D.; Che, D. L.; Liu, C. L.; Ahmed, M.; Leone, S. R.; Worsnop, D. R.; Wilson, K. R. The heterogeneous reaction of hydroxyl radicals with sub-micron squalane particles: a model system for understanding the oxidative aging of ambient aerosols. *Atmos. Chem. Phys.* **2009**, *9* (9), 3209-3222.

(34) Richards-Henderson, N. K.; Goldstein, A. H.; Wilson, K. R. Large enhancement in the heterogeneous oxidation rate of organic aerosols by hydroxyl radicals in the presence of nitric oxide. *J. Phys. Chem. Lett.* **2015**, *6* (22), 4451-4455.
(35) Zhao, Z.; Yang, X.; Lee, J.; Tolentino, R.; Mayorga, R.; Zhang, W.; Zhang, H. Diverse reactions in highly functionalized organic aerosols during thermal desorption. *ACS Earth Space Chem.* **2020**, *4* (2), 283-296.
(36) Zhao, Z.; Tolentino, R.; Lee, J.; Vuong, A.; Yang, X.; Zhang, H. Interfacial dimerization by organic radical reactions during heterogeneous oxidative aging of oxygenated organic aerosols. *J. Phys. Chem. A* **2019**, *123* (50), 10782-10792.
(37) Zhao, Z.; Mayorga, R.; Lee, J.; Yang, X.; Tolentino, R.; Zhang, W.; Vuong, A.; Zhang, H. Site-specific mechanisms in OH-initiated organic aerosol heterogeneous oxidation revealed by isomer-resolved molecular characterization. *ACS Earth Space Chem.* **2020**, *4* (5), 783-794.
(38) Zhao, Z.; Xu, Q.; Yang, X.; Zhang, H. Heterogeneous ozonolysis of endocyclic unsaturated organic aerosol proxies: Implications for Criegee intermediate dynamics and later-generation reactions. *ACS Earth Space Chem.* **2019**, *3* (3), 344-356.
(39) Shen, C.; Zhang, W.; Choczynski, J.; Davies, J. F.; Zhang, H. Phase State and Relative Humidity Regulate the Heterogeneous Oxidation Kinetics and Pathways of Organic-Inorganic Mixed Aerosols. *Environ. Sci. Technol.* **2022**, *56* (22), 15398-15407.
(40) Berndt, T.; Richters, S.; Jokinen, T.; Hyttinen, N.; Kurtén, T.; Otkjær, R. V.; Kjaergaard, H. G.; Stratmann, F.; Herrmann, H.; Sipilä, M.; et al. Hydroxyl radical-induced formation of highly oxidized organic compounds. *Nat. Commun.* **2016**, *7* (1), 13677.
(41) Hunt, D. F.; McEwen, C. N.; Upham, R. A. Determination of active hydrogen in organic compounds by chemical ionization mass spectrometry. *Anal. Chem.* **1972**, *44* (7), 1292-1294.
(42) Damont, A.; Legrand, A.; Cao, C.; Fenaille, F.; Tabet, J.-C. Hydrogen/deuterium exchange mass spectrometry in the world of small molecules. *Mass Spectrom. Rev.* **2023**, *42* (4), 1300-1331.
(43) Kostyukevich, Y.; Acter, T.; Zherebker, A.; Ahmed, A.; Kim, S.; Nikolaev, E. Hydrogen/deuterium exchange in mass spectrometry. *Mass Spectrom. Rev.* **2018**, *37* (6), 811-853.
(44) Zhao, Z.; Le, C.; Xu, Q.; Peng, W.; Jiang, H.; Lin, Y.-H.; Cocker, D. R.; Zhang, H. Compositional evolution of secondary organic aerosol as temperature and relative humidity cycle in atmospherically relevant ranges. *ACS Earth Space Chem.* **2019**, *3* (11), 2549-2558.
(45) Mayorga, R. J.; Zhao, Z.; Zhang, H. Formation of secondary organic aerosol from nitrate radical oxidation of phenolic VOCs: Implications for nitration mechanisms and brown carbon formation. *Atmos. Environ.* **2021**, *244*, 117910.
(46) Docherty, K. S.; Ziemann, P. J. Effects of Stabilized Criegee Intermediate and OH Radical Scavengers on Aerosol Formation from Reactions of β-Pinene with $O_3$. *Aerosol Sci. Technol.* **2003**, *37* (11), 877-891.
(47) Physicochemical and Physical Treatment of Pollutants and Wastes. In *Environmental Chemistry: Fundamentals*, Ibanez, J. G., Hernandez-Esparza, M., Doria-Serrano, C., Fregoso-Infante, A., Singh, M. M. Eds.; Springer New York, 2007; pp 237-275.
(48) Atkinson, R.; Baulch, D. L.; Cox, R. A.; Crowley, J. N.; Hampson, R. F.; Hynes, R. G.; Jenkin, M. E.; Rossi, M. J.; Troe, J.; Subcommittee, I. Evaluated kinetic and photochemical data for atmospheric chemistry: Volume II – gas phase reactions of organic species. *Atmos. Chem. Phys.* **2006**, *6* (11), 3625-4055.
(49) Jenkin, M. E.; Young, J. C.; Rickard, A. R. The MCM v3.3.1 degradation scheme for isoprene. *Atmos. Chem. Phys.* **2015**, *15* (20), 11433-11459.

(50) Jenkin, M. E.; Saunders, S. M.; Wagner, V.; Pilling, M. J. Protocol for the development of the Master Chemical Mechanism, MCM v3 (Part B): tropospheric degradation of aromatic volatile organic compounds. *Atmos. Chem. Phys.* **2003**, *3* (1), 181-193.
(51) Faust, J. A.; Abbatt, J. P. D. Organic Surfactants Protect Dissolved Aerosol Components against Heterogeneous Oxidation. *J. Phys. Chem. A* **2019**, *123* (10), 2114-2124.
(52) Christensen, L. E.; Okumura, M.; Sander, S. P.; Salawitch, R. J.; Toon, G. C.; Sen, B.; Blavier, J. F.; Jucks, K. W. Kinetics of $HO_2 + HO_2 \rightarrow H_2O_2 + O_2$: Implications for Stratospheric $H_2O_2$. *Geophys. Res. Lett.* **2002**, *29* (9), 13-11-13-14.
(53) Crounse, J. D.; Paulot, F.; Kjaergaard, H. G.; Wennberg, P. O. Peroxy radical isomerization in the oxidation of isoprene. *Phys. Chem. Chem. Phys.* **2011**, *13* (30), 13607-13613, 10.1039/C1CP21330J.
(54) Russell, G. A. Deuterium-isotope effects in the autoxidation of aralkyl hydrocarbons. mechanism of the interaction of peroxy radicals[1]. *J. Am. Chem. Soc.* **1957**, *79* (14), 3871-3877.
(55) McCloskey, J. A. [16] Introduction of deuterium by exchange for measurement by mass spectrometry. In *Methods in Enzymology*, Vol. 193; Academic Press, 1990; pp 329-338.
(56) Custer, T. G.; Kato, S.; Fall, R.; Bierbaum, V. M. Negative ion mass spectrometry and the detection of carbonyls and HCN from clover. *Geophys. Res. Lett.* **2000**, *27* (23), 3849-3852.
(57) Enami, S.; Hoffmann, M. R.; Colussi, A. J. In Situ Mass Spectrometric Detection of Interfacial Intermediates in the Oxidation of RCOOH(aq) by Gas-Phase OH-Radicals. *J. Phys. Chem. A* **2014**, *118* (23), 4130-4137.
(58) Krapf, M.; El Haddad, I.; Bruns, Emily A.; Molteni, U.; Daellenbach, Kaspar R.; Prévôt, André S. H.; Baltensperger, U.; Dommen, J. Labile peroxides in secondary organic aerosol. *Chem* **2016**, *1* (4), 603-616.
(59) Pospisilova, V.; Lopez-Hilfiker, F. D.; Bell, D. M.; El Haddad, I.; Mohr, C.; Huang, W.; Heikkinen, L.; Xiao, M.; Dommen, J.; Prevot, A. S. H.; et al. On the fate of oxygenated organic molecules in atmospheric aerosol particles. *Sci. Adv. 6* (11), eaax8922.
(60) Mertes, P.; Pfaffenberger, L.; Dommen, J.; Kalberer, M.; Baltensperger, U. Development of a sensitive long path absorption photometer to quantify peroxides in aerosol particles (Peroxide-LOPAP). *Atmos. Meas. Tech.* **2012**, *5* (10), 2339-2348.
(61) Pagonis, D.; Ziemann, P. J. Chemistry of hydroperoxycarbonyls in secondary organic aerosol. *Aerosol Sci. Technol.* **2018**, *52* (10), 1178-1193.
(62) Paulot, F.; Crounse, J. D.; Kjaergaard, H. G.; Kürten, A.; St. Clair, J. M.; Seinfeld, J. H.; Wennberg, P. O. Unexpected Epoxide Formation in the Gas-Phase Photooxidation of Isoprene. *Science* **2009**, *325* (5941), 730.
(63) St. Clair, J. M.; Rivera-Rios, J. C.; Crounse, J. D.; Knap, H. C.; Bates, K. H.; Teng, A. P.; Jørgensen, S.; Kjaergaard, H. G.; Keutsch, F. N.; Wennberg, P. O. Kinetics and Products of the Reaction of the First-Generation Isoprene Hydroxy Hydroperoxide (ISOPOOH) with OH. *J. Phys. Chem. A* **2016**, *120* (9), 1441-1451.
(64) Mettke, P.; Brüggemann, M.; Mutzel, A.; Gräfe, R.; Herrmann, H. Secondary Organic Aerosol (SOA) through Uptake of Isoprene Hydroxy Hydroperoxides (ISOPOOH) and its Oxidation Products. *ACS Earth Space Chem.* **2023**, *7* (5), 1025-1037.
(65) Surratt, J. D.; Chan, A. W. H.; Eddingsaas, N. C.; Chan, M.; Loza, C. L.; Kwan, A. J.; Hersey, S. P.; Flagan, R. C.; Wennberg, P. O.; Seinfeld, J. H. Reactive intermediates revealed in secondary organic aerosol formation from isoprene. *Proc. Natl. Acad. Sci. U.S.A.* **2010**, *107* (15), 6640.

(66) Zhang, W.; Zhang, H. Secondary ion chemistry mediated by ozone and acidic organic molecules in iodide-adduct chemical ionization mass spectrometry. *Anal. Chem.* **2021**, *93* (24), 8595-8602.
(67) Kurtén, T.; Møller, K. H.; Nguyen, T. B.; Schwantes, R. H.; Misztal, P. K.; Su, L.; Wennberg, P. O.; Fry, J. L.; Kjaergaard, H. G. Alkoxy radical bond scissions explain the anomalously low secondary organic aerosol and organonitrate yields from α-pinene + $NO_3$. *J. Phys. Chem. Lett.* **2017**, *8* (13), 2826-2834.
(68) Zhang, H.; Ruehl, C. R.; Chan, A. W. H.; Nah, T.; Worton, D. R.; Isaacman, G.; Goldstein, A. H.; Wilson, K. R. OH-initiated heterogeneous oxidation of cholestane: A model system for understanding the photochemical aging of cyclic alkane aerosols. *J. Phys. Chem. A* **2013**, *117* (47), 12449-12458.
(69) Nah, T.; Zhang, H.; Worton, D. R.; Ruehl, C. R.; Kirk, B. B.; Goldstein, A. H.; Leone, S. R.; Wilson, K. R. Isomeric Product Detection in the Heterogeneous Reaction of Hydroxyl Radicals with Aerosol Composed of Branched and Linear Unsaturated Organic Molecules. *J. Phys. Chem. A* **2014**, *118* (49), 11555-11571.
(70) Chan, M. N.; Zhang, H.; Goldstein, A. H.; Wilson, K. R. Role of water and phase in the heterogeneous oxidation of solid and aqueous succinic acid aerosol by hydroxyl radicals. *J. Phys. Chem. C* **2014**, *118* (50), 28978-28992.
(71) Crehuet, R.; Anglada, J. M.; Bofill, J. M. Tropospheric Formation of Hydroxymethyl Hydroperoxide, Formic Acid, $H_2O_2$, and OH from Carbonyl Oxide in the Presence of Water Vapor: A Theoretical Study of the Reaction Mechanism. *Chem. Eur. J.* **2001**, *7* (10), 2227-2235.
(72) Zhao, R.; Kenseth, C. M.; Huang, Y.; Dalleska, N. F.; Kuang, X. M.; Chen, J.; Paulson, S. E.; Seinfeld, J. H. Rapid aqueous-phase hydrolysis of ester hydroperoxides arising from criegee intermediates and organic acids. *J. Phys. Chem. A* **2018**, *122* (23), 5190-5201.
(73) Dyson, J. E.; Whalley, L. K.; Slater, E. J.; Woodward-Massey, R.; Ye, C.; Lee, J. D.; Squires, F.; Hopkins, J. R.; Dunmore, R. E.; Shaw, M.; et al. Impact of HO2 aerosol uptake on radical levels and $O_3$ production during summertime in Beijing. *Atmos. Chem. Phys.* **2023**, *23* (10), 5679-5697.
(74) Brune, W. H.; Tan, D.; Faloona, I. F.; Jaeglé, L.; Jacob, D. J.; Heikes, B. G.; Snow, J.; Kondo, Y.; Shetter, R.; Sachse, G. W.; et al. OH and $HO_2$ chemistry in the North Atlantic free troposphere. *Geophys. Res. Lett.* **1999**, *26* (20), 3077-3080.
(75) Jaeglé, L.; Jacob, D. J.; Brune, W. H.; Faloona, I.; Tan, D.; Heikes, B. G.; Kondo, Y.; Sachse, G. W.; Anderson, B.; Gregory, G. L.; et al. Photochemistry of HO x in the upper troposphere at northern midlatitudes. *J. Geophys. Res.: Atmos.* **2000**, *105* (D3), 3877-3892.
(76) Olson, J. R.; Crawford, J. H.; Chen, G.; Fried, A.; Evans, M. J.; Jordan, C. E.; Sandholm, S. T.; Davis, D. D.; Anderson, B. E.; Avery, M. A.; et al. Testing fast photochemical theory during TRACE-P based on measurements of OH, $HO_2$, and $CH_2O$. *J. Geophys. Res.: Atmos.* **2004**, *109* (D15).
(77) Olson, J. R.; Crawford, J. H.; Chen, G.; Brune, W. H.; Faloona, I. C.; Tan, D.; Harder, H.; Martinez, M. A reevaluation of airborne $HO_x$ observations from NASA field campaigns. *J. Geophys. Res.: Atmos.* **2006**, *111* (D10).
(78) Pöschl, U.; Shiraiwa, M. Multiphase chemistry at the atmosphere–biosphere interface influencing climate and public health in the anthropocene. *Chem. Rev.* **2015**, *115* (10), 4440-4475.
(79) Kleindienst, T. E.; Lewandowski, M.; Offenberg, J. H.; Jaoui, M.; Edney, E. O. The formation of secondary organic aerosol from the isoprene + OH reaction in the absence of $NO_x$. *Atmos. Chem. Phys.* **2009**, *9* (17), 6541-6558.